Article

Developmental Cell

Specification of Dendritogenesis Site in *Drosophila* aCC Motoneuron by Membrane Enrichment of Pak1 through Dscam1

Graphical Abstract

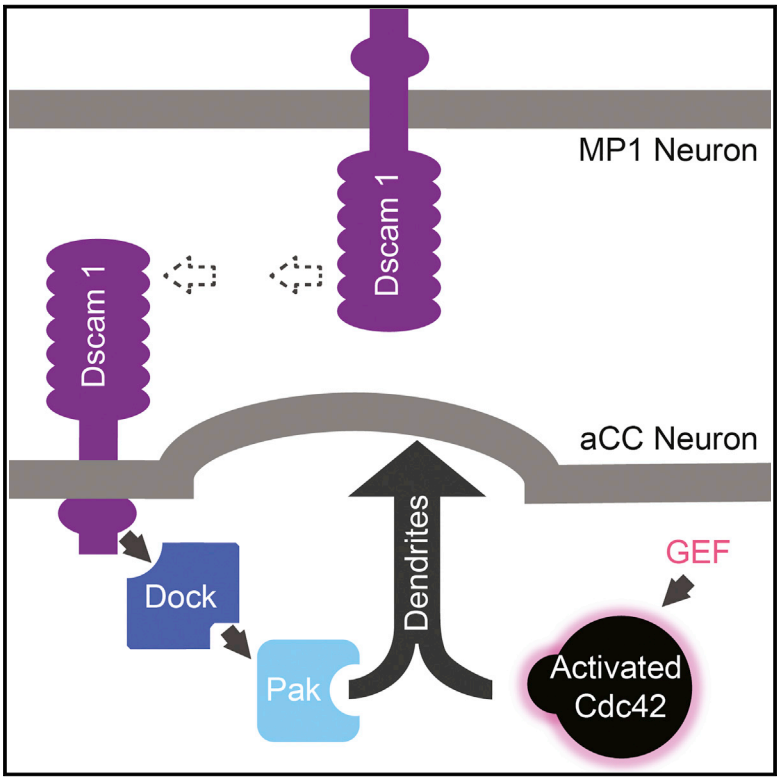

Highlights

- Dendrites grow where Pak1 membrane accumulation and Cdc42 activation coincide
- Pak is localized to the membrane by Dscam1 through Dock, independent of Cdc42
- Interneuron contact involving Dscam1 guides Dscam1 localization in aCC
- Dscam1 defines the dendrogenesis site by spatially confining Cdc42 signaling

Authors

Daichi Kamiyama, Ryan McGorty, Rie Kamiyama, Michael D. Kim, Akira Chiba, Bo Huang

Correspondence

daichi.kamiyama@ucsf.edu (D.K.), bo.huang@ucsf.edu (B.H.)

In Brief

Proper neuronal wiring requires precise positioning of dendritic branches. Kamiyama et al. show that a Dscam1-Dock-Pak1 hierarchical interaction defines the site of dendritogenesis in the aCC motoneuron in *Drosophila*, in part via Dscam1-dependent inter-neuronal interactions that specify Dscam1 localization in aCC.

Kamiyama et al., 2015, Developmental Cell *35*, 93–106
October 12, 2015
http://dx.doi.org/10.1016/j.devcel.2015.09.007

CellPress

Developmental Cell
Article

Specification of Dendritogenesis Site in *Drosophila* aCC Motoneuron by Membrane Enrichment of Pak1 through Dscam1

Daichi Kamiyama,[1,*] Ryan McGorty,[1] Rie Kamiyama,[1] Michael D. Kim,[3,4] Akira Chiba,[2,3] and Bo Huang[1,5,*]
[1]Department of Pharmaceutical Chemistry, University of California, San Francisco, San Francisco, CA 94158, USA
[2]Department of Biology, University of Miami, Coral Gables, FL 33146, USA
[3]Miami Institute of Molecular Imaging and Computation, Coral Gables, FL 33146, USA
[4]Department of Molecular and Cellular Pharmacology, Miller School of Medicine, University of Miami, Miami, FL 33136, USA
[5]Department of Biochemistry and Biophysics, University of California, San Francisco, San Francisco, CA 94158, USA
*Correspondence: daichi.kamiyama@ucsf.edu (D.K.), bo.huang@ucsf.edu (B.H.)
http://dx.doi.org/10.1016/j.devcel.2015.09.007

SUMMARY

Precise positioning of dendritic branches is a critical step in the establishment of neuronal circuitry. However, there is limited knowledge on how environmental cues translate into dendrite initiation or branching at a specific position. Here, through a combination of mutation, RNAi, and imaging experiments, we found that a Dscam-Dock-Pak1 hierarchical interaction defines the stereotypical dendrite growth site in the *Drosophila* aCC motoneuron. This interaction localizes the Cdc42 effector Pak1 to the plasma membrane at the dendrite initiation site before the activation of Cdc42. Ectopic expression of membrane-anchored Pak1 overrides this spatial specification of dendritogenesis, confirming its function in guiding Cdc42 signaling. We further discovered that Dscam1 localization in aCC occurs through an interneuronal contact that involves Dscam1 in the partner MP1 neuron. These findings elucidate a mechanism by which Dscam1 controls neuronal morphogenesis through spatial regulation of Cdc42 signaling and, subsequently, cytoskeletal remodeling.

INTRODUCTION

A choreographed sequence of cellular interactions through multiple signaling events takes place when the axon and dendrites of individual neurons are sculptured during the establishment of the nervous system (Cheng and Poo, 2012; Dickson, 2002; Jan and Jan, 2003). Compared to what we have learned about axon outgrowth and guidance (Vitriol and Zheng, 2012), our knowledge on the regulation of dendritic development is limited (Jan and Jan, 2010), partially because of the more complicated morphologies and the smaller size of dendritic branches. Although the shapes of dendrites may appear to be random, many model systems have illustrated that dendrite growth could be under strict spatial-temporal control. This regulation is essential for the correct wiring of neuronal circuitries during development (Sanes and Zipursky, 2010; Yogev and Shen, 2014). The importance in inter-cellular contact signaling to dendrite morphogenesis has been recently demonstrated in the *C. elegans* sensory PVD neuron, in which the ligand complex SAX7/MNR-1 from hypodermis cells spatially activates DMA-1 on the neurites and consequently leads to the formation of branches at the contact point (Dong et al., 2013, 2015; Salzberg et al., 2013). Still, how these types of external spatial cues translate into dendrite morphogenesis through the regulation of cytoskeletal activity has yet to be fully elucidated. To investigate such molecular mechanisms, we chose the aCC (anterior corner cell) motoneuron in the *Drosophila* embryonic CNS because of its highly stereotyped yet simple dendrite development (Figure 1A). In the CNS neuropil, the aCC sprouts its dendrites as collateral processes from the axon exactly 13 μm from the midline at hour 13:00 after egg laying (AEL) of embryogenesis (Figure 1A). This process is largely invariant and thus ideal for studying the molecular mechanisms that govern the precise spatiotemporal positioning of dendrite outgrowth in the CNS (Kamiyama and Chiba, 2009).

During neuronal morphogenesis, spatial and temporal signals from multiple intracellular and extracellular sources are integrated to trigger a sequence of activities in membrane trafficking and cytoskeleton rearrangement (Alberts, 1998; Alberts et al., 2007). At the intersection of these signaling pathways, Cdc42, a member of the Rho family of small GTPases, is particularly important (Etienne-Manneville and Hall, 2002). Cdc42 cycles between guanosine diphosphate-associated inactive and guanosine triphosphate-associated active states, reciprocally controlled by GTPase-activating proteins (GAPs) and guanine nucleotide exchange factors (GEFs). Activated Cdc42 can bind dozens of effectors that regulate cytoskeletal dynamics and vesicle trafficking (Etienne-Manneville, 2004; Etienne-Manneville and Hall, 2002; Hall, 1998). How Cdc42 signaling leads to cell morphogenesis with spatial, temporal, and pathway precision is a question under intensive study (Etienne-Manneville, 2004; Etienne-Manneville and Hall, 2002; Mogilner et al., 2012; Murakoshi et al., 2011; Welch et al., 2011). Many functions of *cdc42* are conserved across phyla (Govek et al., 2005, 2011; Hall and Lalli, 2010; Luo, 2000) and loss of *cdc42* function leads to neuron development defects in both vertebrates and invertebrates (Garvalov et al., 2007). In the *Drosophila* aCC motoneuron, the

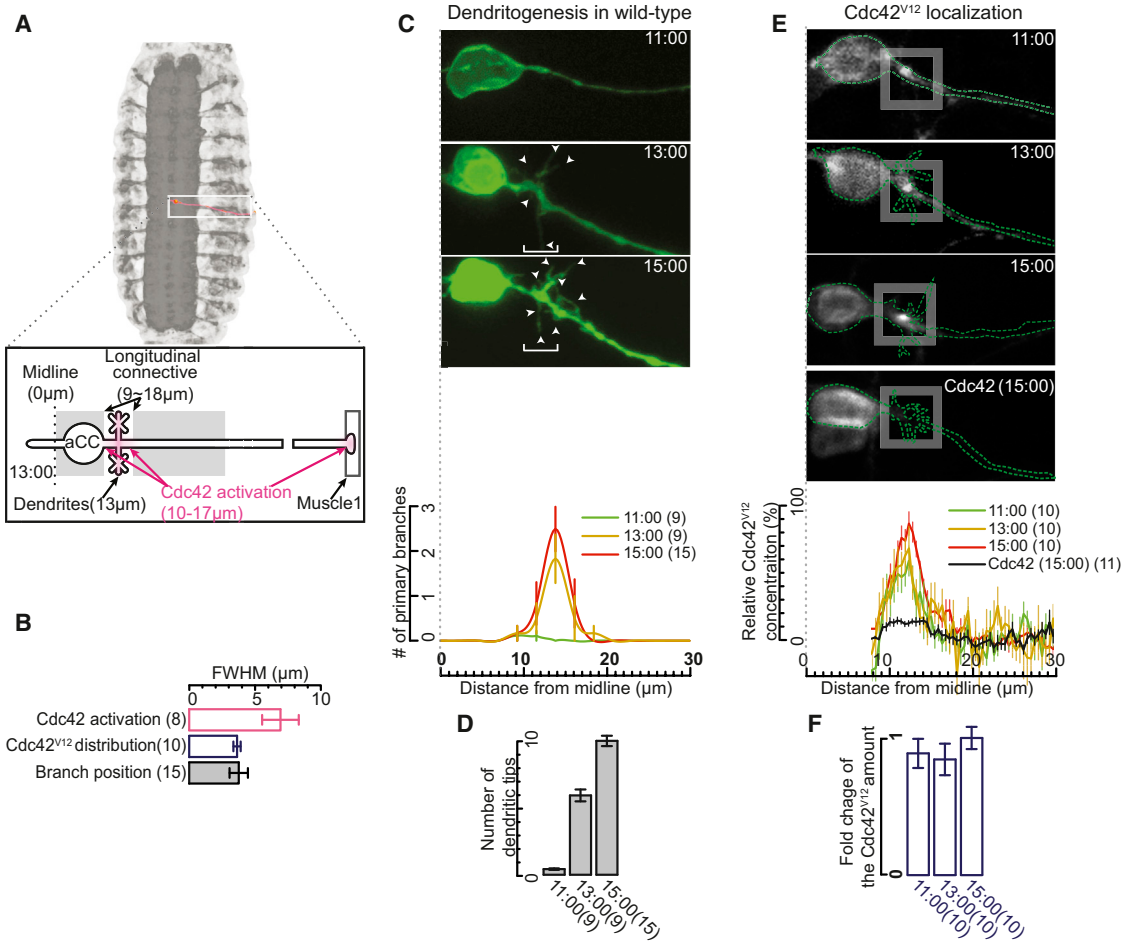

Figure 1. GFP::Cdc42^{V12} Accumulation Spatially Corresponds with the aCC Dendritogenesis Site

(A) In each half-segment of an embryo, aCC motoneurons begin to develop their dendrites at a stereotyped position within the CNS, where its axon intersects with the longitudinal connective.

(B) The distribution FWHMs for Cdc42 activation, GFP::Cdc42^{V12} accumulation, and primary dendritic branches' positions. The sample size (*n*) is the number of aCCs examined in abdominal segments from A2 to A5.

(C) Representative images of lipophilic-dye-labeled aCC aligned to the CNS midline (dashed line) from 11:00 to 15:00 in a wild-type strain. The distribution of primary dendritic branches is also plotted (bottom).

(D) The mean number of dendritic tips from 11:00 to 15:00.

(E) GFP::Cdc42^{V12} is localized at the base of the primary branches (inset). The mean of relative GFP::Cdc42^{V12} fluorescence 10 to 30 μm from the midline is shown. Their concentrations are normalized to the average concentrations in the aCC cell body. GFP::Cdc42 localization at 15:00 was used as a control.

(F) Quantification of the GFP::Cdc42^{V12} amount 10 to 30 μm from the midline at the indicated hours versus at 15:00. Error bars, SEM.

See also Figure S1 and Table S1.

dendritogenesis process cell-autonomously requires *cdc42* function (Kamiyama and Chiba, 2009; Figure S1A) but not the *rac* genes (*rac1/rac2/mtl* loss-of-function mutations display less severe defects; see Figure S1A). To further elucidate the mechanism by which Cdc42 controls dendrite outgrowth, we previously introduced a Cdc42 activation probe (aProbe; Kamiyama and Chiba, 2009) based on intramolecular fluorescence resonance energy transfer. We found that Cdc42 remains inactive in aCC before hour 13:00 AEL, the onset time point of dendrite outgrowth. Although the timing of Cdc42 activation coincides with that of dendrite outgrowth in aCC, the region of Cdc42 activation is too large to account for the precise dendrite positioning (Figures 1A and 1B). This discrepancy led us to speculate that other mechanisms may be present to restrict Cdc42 signaling to the site of dendrite initiation. For example, in the establishment of cell polarity, the restricted subcellular localization of Cdc42 interaction partners, e.g., its effectors, is a key to confine Cdc42 signaling (Kozubowski et al., 2008; Park and Bi, 2007; Slaughter et al., 2009).

In this paper, we combine RNAi screening, knockout verification, high-resolution structured illumination microscopy (SIM) imaging, and gain-of-function studies to show that the local enrichment of Cdc42 effectors, especially the localization of p21 protein Cdc42/Rac-activated kinase (Pak1) to the plasma membrane, is the mechanism that specifies the dendritogenesis site in aCC. Inspired by previous genetic and biochemical

studies that indicated the role of the Dscam1/Dock/Pak signaling pathway in regulating axon guidance in *Drosophila* (Hing et al., 1999; Schmucker et al., 2000), we further demonstrate that Down syndrome cell-adhesion molecule (Dscam1) functions as the cell surface receptor that recruits Pak1 to the membrane via Dreadlocks (Dock) and this recruitment occurs independent of Cdc42 activity. Finally, we discover that the external spatial cue for Dscam1 localization in aCC comes from contact with the MP1 pioneer neuron. Our findings provide mechanistic evidence that Dscam1 regulates neuronal morphogenesis through the spatial regulation of Cdc42 signaling and therefore cytoskeletal remodeling.

RESULTS

Cdc42 Effector Accumulation Coincides Spatially with aCC Dendritogenesis

To quantitatively characterize dendritogenesis in the aCC motoneuron, we imaged its morphology by lipophilic-dye labeling. From 11:00 to 15:00 AEL, we quantified the position of primary dendritic branches defined as their distances to the midline (Figure 1C), as well as the number of all dendritic tips (Figure 1D). These measurements indicate that the initiation of dendrite outgrowth starts at 12.9 ± 0.3 μm (mean ± SEM) from the midline at 13:00 AEL. The full width at half maximum (FWHM) of primary branch position distribution was 3.9 ± 0.9 μm (mean ± SEM). In contrast, the region of Cdc42 activation, as indicated by the FWHM of the aProbe signal at 13:00 AEL, was measured to be 6.8 ± 1.0 μm (mean ± SEM) in our previous study (Figure 1B; Kamiyama and Chiba, 2009).

To identify the interaction partners of Cdc42 in aCC, we took an imaging-based approach adapted from previous in vitro and in vivo protein-Cdc42 interaction assays (Formstecher et al., 2005) using a constitutively active mutant of Cdc42, $Cdc42^{V12}$ (Aceto et al., 2006; Formstecher et al., 2005; Owen et al., 2000). To gain single-neuron resolution, we used an *eve′-GAL4* driver to express $Cdc42^{V12}$ tagged with GFP (GFP::$Cdc42^{V12}$; Figure S1A) selectively in aCC and its sibling pCC and RP2 neurons (Figure S1B). To avoid the potential artifacts from continuous $Cdc42^{V12}$ expression, we used an inducible expression system to briefly express the transgene for 3 hr before the time point of imaging (Figures S1B and S1C). No obvious defects in cell body migration, axon growth or guidance (Figure S1B and S1C), or aCC dendritic branch number (Figure S1D) were observed in this case. We performed immunostaining with anti-Cdc42 antibodies to confirm that the expression level of GFP::$Cdc42^{V12}$ was comparable to that of endogenous Cdc42 (Figures S1E and S1F).

We characterized the pattern of GFP::$Cdc42^{V12}$ accumulation along the aCC axon from 11:00 to 15:00 AEL. GFP::$Cdc42^{V12}$ accumulation at the dendritogenesis site was found to precede Cdc42 activation by at least 2 hr (Figures 1E and 1F). Interestingly, the width of GFP::$Cdc42^{V12}$ accumulation (3.7 ± 0.3 μm, mean ± SEM; Figure 1B) matched that of the dendrite outgrowth region. In contrast, GFP::Cdc42 under the same expression control showed a flat distribution in the same region (Figure 1E), indicating that the accumulation of $Cdc42^{V12}$ is specific to the interaction between activated Cdc42 and its binding partners. Therefore, we reasoned that the local enrichment of the Cdc42 interaction partners might be responsible for positioning dendrite outgrowth. Despite our efforts to minimize $Cdc42^{V12}$ expression, there is still a risk of potential artifacts caused by constitutively activating Cdc42. Therefore, in subsequent experiments, GFP::$Cdc42^{V12}$ was only used as a screening readout to identify the Cdc42 interaction partners responsible for aCC dendritogenesis.

Pak1, along with Several Other Cdc42 Effectors, Is Responsible for GFP::$Cdc42^{V12}$ Accumulation and aCC Dendritogenesis

To narrow down candidates for Cdc42 interaction partners enriched at the dendrite outgrowth site, we tested a mutant of $Cdc42^{V12}$, $Cdc42^{V12C40}$, for which a mutation at Tyr40 disrupts its binding to partners containing the Cdc42/Rac-interactive binding (CRIB) motif (Burbelo et al., 1995; Manser et al., 1994; Owen et al., 2000). GFP::$Cdc42^{V12C40}$ did not accumulate at the dendritogenesis site (Figure 2A), suggesting that interaction partners at the site likely contain the CRIB motif.

Drosophila has nine putative CRIB-containing genes for Cdc42: *Pak1*, *Pak2*, *Pak3*, *MRCK* (myotonic dystrophy kinase-related Cdc42-binding kinase), *Mlk* (mixed lineage kinase), *Flk* (Fak-like kinase), *WASp* (Wiskott-Aldrich syndrome protein), *Par6* (partitioning-defective protein 6), and *Spec* (small binding proteins for Cdc42). By injecting double-stranded RNA (dsRNA) at the syncytial blastoderm stage (Kennerdell and Carthew, 1998), we knocked down each of these genes in embryos expressing GFP::$Cdc42^{V12}$ in aCC. Knocking down *Flk*, *Pak1*, *Pak2*, *MRCK*, *Mlk*, *WASp*, *Par6*, or *Spec* caused a small but significant reduction in GFP::$Cdc42^{V12}$ accumulation at the region of dendrite growth (Figure 2A).

To validate these identified candidates and their function in aCC, we examined the dendrite tip number by knocking down each one of them with the aCC-specific expression of short hairpin RNA (shRNA) using established *UAS-shRNA* lines. Knocking down *Pak1*, *MRCK*, *Flk*, or *WASp* led to a significant reduction in the dendrite tip number (Figure 2B). The incomplete suppression of dendritogenesis in the individual knockdowns implied a functional redundancy among these genes, which was confirmed by the drastic reduction in the dendrite branch number (~80%) when all four dsRNA constructs (*Pak1*, *MRCK*, *Flk*, and *WASp*) were co-injected into embryos (Figure 2B). Among these four effectors, knocking down *Pak1* caused the greatest reduction in the dendrite tip number. To further confirm the function of *Pak1*, we imaged aCC dendritogenesis in embryos homozygous for a loss-of-function mutation in *pak1*, revealing a significant decrease in the dendrite tip number (Figure 2C). Resupplying the *Pak1* gene back only to aCC rescued this phenotype (Figure 2C), suggesting that *Pak1* is cell-autonomously required for aCC dendritogenesis.

Pak1 Is Enriched at the Ventral Plasma Membrane of the aCC Dendritogenesis Site

As a complimentary approach to genetic perturbation, we assessed the involvement of Pak1 at the aCC dendritogenesis site by direct microscopy observation. Although it is desirable to image endogenous Pak1, e.g., by anti-Pak1 immunohistochemistry, such studies are challenging because of the ubiquitous presence of Pak1 in cells that tangle around the aCC dendritogenesis site

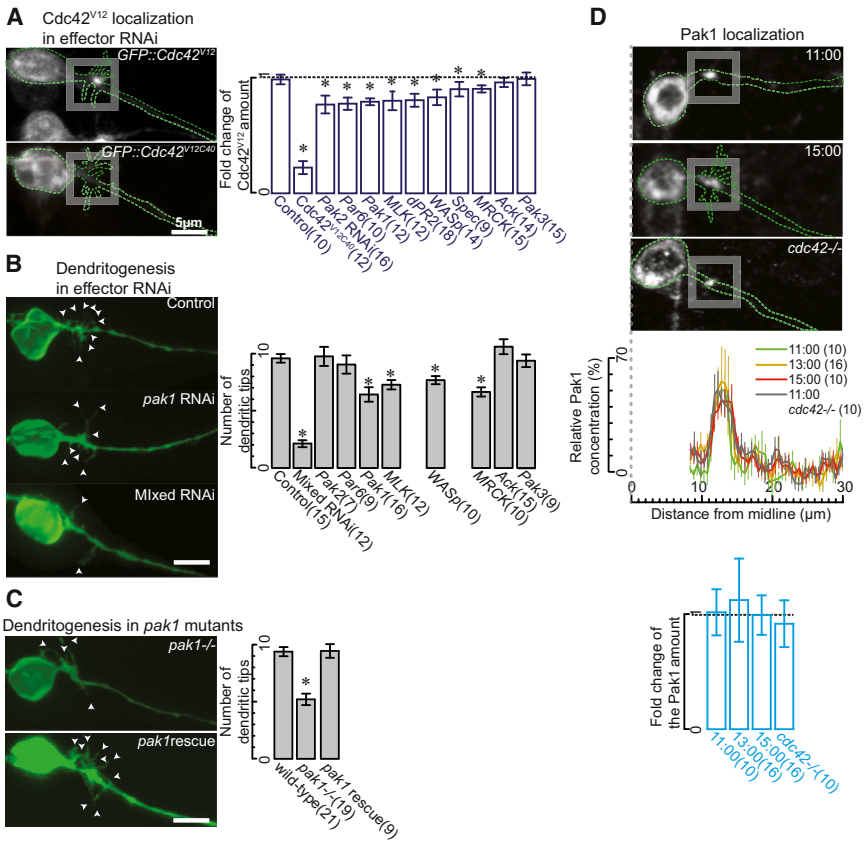

Figure 2. Pak1 Is Required for GFPCdc42^{V12} Accumulation, as well as aCC Dendritogenesis

(A) Images of GFP::Cdc42^{V12} and GFP::Cdc42^{V12C40} localization in aCC at 15:00. As opposed to GFP::Cdc42^{V12}, GFP::Cdc42^{V12C40} failed to accumulate at the aCC dendritogenesis site. We quantified the amount of GFP::Cdc42^{V12} with dsRNA injection. Compared to the sham-operated control (an empty vector injection), GFP::Cdc42^{V12} accumulation at the site is reduced (*$p < 0.005$ by two-tailed t test).

(B) Expression of RNAi constructs or injection of mixed RNAi constructs caused significant reduction of the number of dendritic tips in aCC at 15:00 (*$p < 0.001$ compared with *eve′-GAL4*$^{/+}$, the control, alone by two-tailed t test).

(C) Loss-of-function mutants of *pak1*$^{-/-}$ reduce the dendritic tip number in aCC. The phenotype is rescued by resupplying the wild-type *pak1* gene to aCC (*$p < 0.005$ compared with the one in a wild-type background at 15:00 by two-tailed t test).

(D) Representative images of Pak1 localization in aCC at 11:00 and 15:00. Pak1 is pre-localized where the dendrites normally start to sprout at 11:00. Pak1 localization at 11:00 was not affected even in *cdc42*$^{-/-}$ mutants. Bottom: quantification of the Pak1 amount 10 to 30 μm from the midline in the indicated hours and genotypes versus the one at 15:00. Error bars, SEM.

See also Figure S2 and Tables S1 and S2.

(Figure S2A). To solve this problem, we expressed an epitope-tagged Pak1 under the *eve′-GAL4* driver at a near-physiological level (Figure S2B) so that we could perform cell-specific immunofluorescence imaging. A number of tags were tested, and the fluorescent protein mEOS2 was chosen for this purpose. We verified that this additional expression of Pak1::mEOS2 did not alter aCC dendrite development (Figure S2C). In confocal images, Pak1 was found to be enriched at the site where the dendrites normally start to form. Such a restricted localization of Pak1 started 2 hr before the onset of dendritogenesis (Figure 2D), spatiotemporally matching the GFP::Cdc42^{V12} accumulation pattern but not the Cdc42 activation pattern in aCC. In addition, in *cdc42*$^{-/-}$ flies at 11:00 AEL, Pak1 in aCC showed exactly the same accumulation pattern as in wild-type flies (Figure 2D). This result provides strong evidence that regulation of the Pak1 accumulation is independent of Cdc42 activity.

To rigorously assess the subcellular localization of Pak1 at the aCC dendritogenesis site, we used the high-resolution microscopy technique of SIM (Heintzmann and Gustafsson, 2009), because the diameter of the aCC axon (300∼1000 nm) is too small for confocal microscopy (Lichtman and Denk, 2011; McGorty et al., 2013). With spatial resolutions of ∼100 nm in the xy directions and ∼250 nm in the z direction (Gustafsson et al., 2008), 3D SIM allowed us to distinguish cytoplasm versus plasma membrane in the axon cross section (Figure 3A). Our SIM images showed that Pak1 is dispersed in the cytoplasm in the aCC axon away from the dendritogenesis site (Figure 3B), consistent with Pak1 being devoid of membrane-anchoring domains (Bokoch, 2003). However, at the dendrite outgrowth site (13 μm from the midline), Pak1 is enriched on the plasma membrane 2 hr before the onset of dendritogenesis (Figure 3B). Moreover, Pak1 is asymmetrically distributed on the axonal membrane toward the ventral side (Figure 3B). Such asymmetric membrane localization matches the asymmetric dorsal-ventral positioning of primary dendritic branches (Figure 3C).

Forced Membrane Anchoring of Pak1 Overrides the Spatial Confinement of aCC Dendritogenesis

Our microscopy observations suggest a direct role of Pak1 recruitment to the plasma membrane in specifying the site of aCC dendrite outgrowth. This hypothesis is supported by our genetic studies that *pak1* null mutants show not only reduction of the dendritic branch number but also abnormal positioning of the remaining dendrites (Figure 4A). To further test our hypothesis, we expressed in aCC myristoylation-tagged Pak1 (*UAS-Pak1*^{myr}) that is synthetically tethered to the plasma membrane (Hing et al., 1999; Hughes et al., 2007; Lu et al., 1997). We found that the initiation time of aCC dendrites remained unchanged at 13:00 AEL. However, the region containing primary dendritic processes expanded to a FWHM of 9.0 ± 1.2 μm (mean ± SEM) along the axon, without supernumerary dendritic processes appearing beyond this compartment (Figure 4A). The expanded region of dendrites matched the width of the region in which Cdc42 is normally activated (6.8 ± 1.0 μm, mean ± SEM; Figure 4B). To rule out that these extra dendrites are caused by higher doses of Pak1, we imaged aCC with

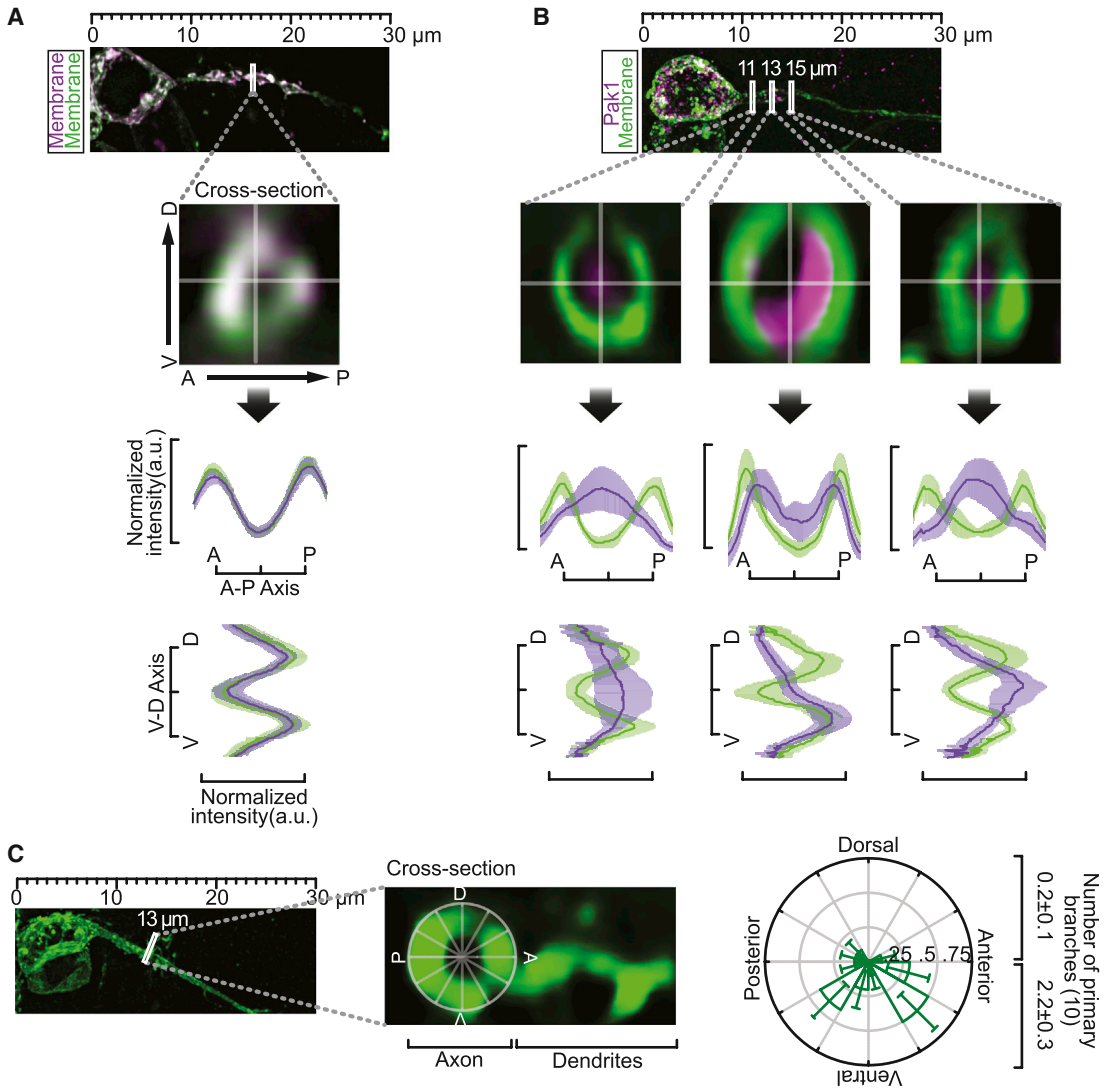

Figure 3. Pak1 Is Enriched at the Ventral Membrane of the aCC Dendritogenesis Site

(A) 3D SIM of the aCC expressing membrane marker, its cross-sectional view, and averaged, normalized slices along the anterior-posterior (A-P) axis and dorsal-ventral (D-V) axis (shades represent SDs, n = 8). The membrane marker is stained with both Alexa Fluor 488 (green) and Alexa Fluor 555 (magenta). Full co-localization in the cross sections demonstrates our capability to precisely align two-color SIM images.

(B) 3D SIM of Pak1 before aCC dendritogenesis at 11:00 (n = 10), showing cross-sectional views 11, 13, and 15 μm from the midline. Pak1 accumulates at the ventral-proximal half of the juxta-membrane at 13 μm but not at 11 or 15 μm. The two separated color channels are also shown in Figure S2D.

(C) 3D SIM of aCC dendrites and its cross-sectional view 13 μm from the midline at 15:00 in wild-type embryos. Radial distribution of primary dendrites, heavily biased to the ventral side, is measured from the center of the axonal cross section to the base of the primary dendrite branches.

See also Figure S2 and Table S1.

overexpression of wild-type Pak1. Dendrite initiation with wild-type Pak1 overexpression was normal, spanning a FWHM of 3.7 ± 0.7 μm (mean ± SEM) along the axons (Figure 4A). This result confirms that the membrane recruitment of Pak1 is sufficient to induce aCC dendrite growth.

Dscam1 and Dock Are Enriched at the aCC Dendritogenesis Site and Critical for aCC Dendritogenesis

The observation that Pak1 accumulates at the ventral membrane, but not at the dorsal-side membrane (Figure 3B), favors a positional cue from cell-cell contact. If Pak1 distribution were to be guided by intracellular signaling or diffusive signaling molecules, we would expect a more symmetric accumulation of Pak1 around the axonal cross section given its small dimension. Previous biochemical data revealed that Pak1 interacts with the SH2-SH3 domain adaptor protein Nck (Hing et al., 1999), whose *Drosophila* ortholog is Dock. Dock interacts with the cytoplasmic domain of the cell-surface receptor Dscam1 (Schmucker et al., 2000). It is thus conceivable that Dscam1, together with Dock, recruits Pak1 to the membrane at the aCC dendritogenesis site. Consistent with this model, we observed diminished

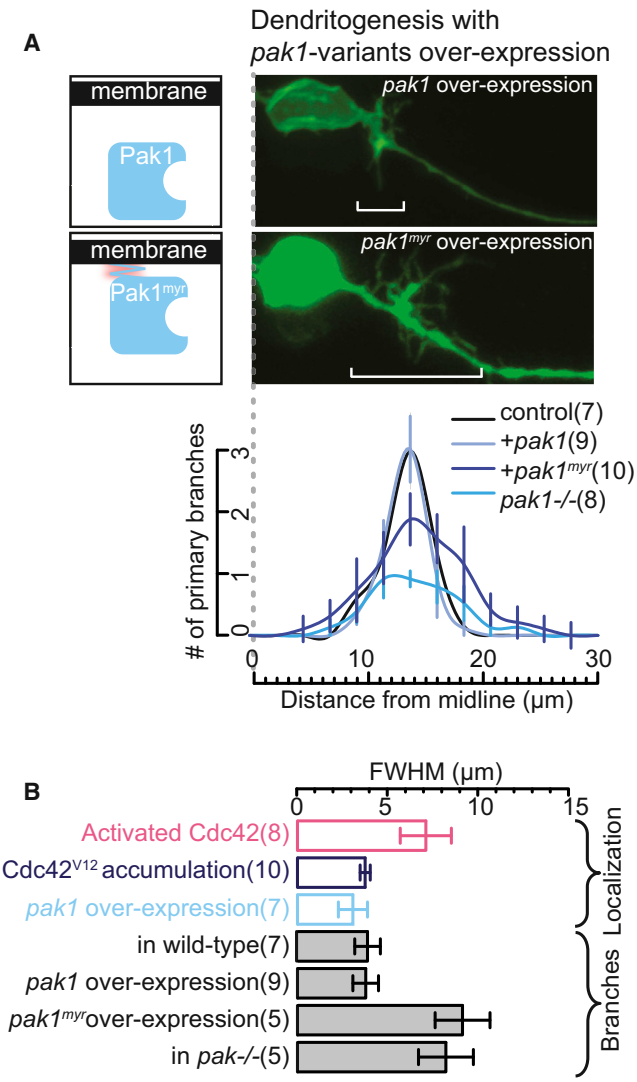

Figure 4. Membrane Tethering of Pak1 Determines the Position of Dendrite Outgrowth

(A) Compared with *eve′-GAL4*$^{/+}$ (control), the *Pak1* mutations caused irregular distribution of primary dendritic branches in aCC (representative images of aCC in a wild-type and a *pak1*$^{-/-}$ mutant background are shown in Figures 1B and 2C, respectively). Although continuous overexpression of *pak1* induces no change from the control, myristoylated Pak1 (*pak1*^{myr}) expression induces expansion of the dendrite outgrowth region with normal dendritogenesis timing.

(B) Summary of the distribution FWHMs for Cdc42 activation, GFP::Cdc42^{V12} accumulation, and Pak1 accumulation, as well as for the dendrite positions in a wild-type, a *pak1* overexpression, a membrane tethered *pak1*^{myr} overexpression, and a *pak1*$^{-/-}$ mutant background. Error bars, SEM.

See also Figure S3 and Table S1.

numbers of aCC dendritic processes in embryos homozygous for *dock* or *dscam1* mutation (Figure 5A), even though the aCC axon extends and targets normally at this development stage. Similar to the *pak1*$^{-/-}$ case, the remaining dendrites were also displaced (Figure 5A). Resupplying the *dock* gene back only to aCC fully rescued the phenotype in the mutant (Figure 5A), indicating a cell-autonomous function of *dock*. However, resupplying a single isoform of *dscam1* (*UAS-Dscam[exon 17.2]-GFP*; Wang et al., 2004) specifically to aCC in the mutant background could not rescue the dendrite number, and the primary branches were still misplaced (Figure 5A). We picked this Dscam1 isoform with an axon-guiding transmembrane domain because the process occurs before dendritogenesis. We have previously verified its expression and axonal localization in aCC (Hsu et al., 2009). Taken together, these results suggest that *dscam1* in other cells is likely involved in this process, either directly in an isoform-specific manner (Wojtowicz et al., 2004, 2007) or indirectly in an isoform-non-specific manner.

Complementary to our epistasis analysis, we performed a genetic interaction assay to validate our *dscam1-dock-pak1* pathway (Schmucker et al., 2000). We found ~40% reduction of the dendrite tip number in the *dock/dscam1* or *pak1/dscam1* transheterozygous mutant compared to the number in the *dock*$^{-/+}$, *dscam1*$^{-/+}$, or *pak1*$^{-/+}$ heterozygous mutant alone (Figure S3). These synergistic genetic interactions among *dscam1*, *dock*, and *pak1* support their function in the same linear pathway. We further verified the direct involvement of the *pak1-dock* interaction using a *pak1* allele (*pak1*^{4}) containing a L9P mutation that disrupts Pak1-Dock binding (Hing et al., 1999). The dendrite tip number in *pak1*^{4}/*pak1*$^{-}$ was significantly lower than that in *pak1*$^{-/+}$ and indistinguishable from that in *pak1*$^{-/-}$ (Figure S3). This result strongly supports the involvement of a specific Dock-Pak1 interaction in signaling aCC dendritogenesis.

If Dscam1 and Dock in aCC directly participate in regulating dendritogenesis, they should be present at the site. To image the temporal and spatial distribution of Dock, we expressed epitope-tagged Dock (*UAS-SNAP::Dock*) in the aCC neurons at a near-physiological level without changing the morphology of the aCC (Figures S4C and S4D). To perform single-neuron imaging of Dscam1 without altering its splicing pattern, we used GFP intron trap insertion into the *dscam1* locus (hereafter named *Dscam1*^{MiMICGFP}) and expressed specifically in aCC anti-GFP nanobodies tagged with mCherry (*mCherry::vhhGFP4*; Venken et al., 2011; Figures S5A–S5C). The mCherry signal reliably indicates where endogenous Dscam1 is enriched in the aCC axon, because a localized mCherry signal at the aCC dendritogenesis site disappeared either with *dscam1* RNAi or in wild-type embryos with only nanobody expression (Figure S5D). Our imaging results showed that both Dock and Dscam1 were enriched at the aCC dendrogenesis site at least 2 hr before the dendrites started to grow (Figures 5B and 5C). The width of Dock or Dscam1 distribution matches that of Pak1 distribution (3.7 ± 0.7 μm with Pak1, 3.6 ± 1.1 μm with Dock, and 4 ± 0.2 μm with Dscam1, mean ± SEM; Figure 5D).

Dscam1 via Dock Recruits Pak1 to the aCC Dendritogenesis Site

With the imaging assay that we have established for Dscam1, Dock, and Pak1 accumulation, we sought to establish their interaction hierarchy. If Dscam1, Dock, and Pak1 function through the same hierarchical pathway, knocking down or out any component in this pathway would abolish the localization of only downstream components, not upstream ones. Our imaging results matched this prediction. Pak1 accumulation at the aCC dendritogenesis site was significantly reduced in *dock*$^{-/-}$ or *dscam1* RNAi embryos. Dock accumulation was also significantly reduced in

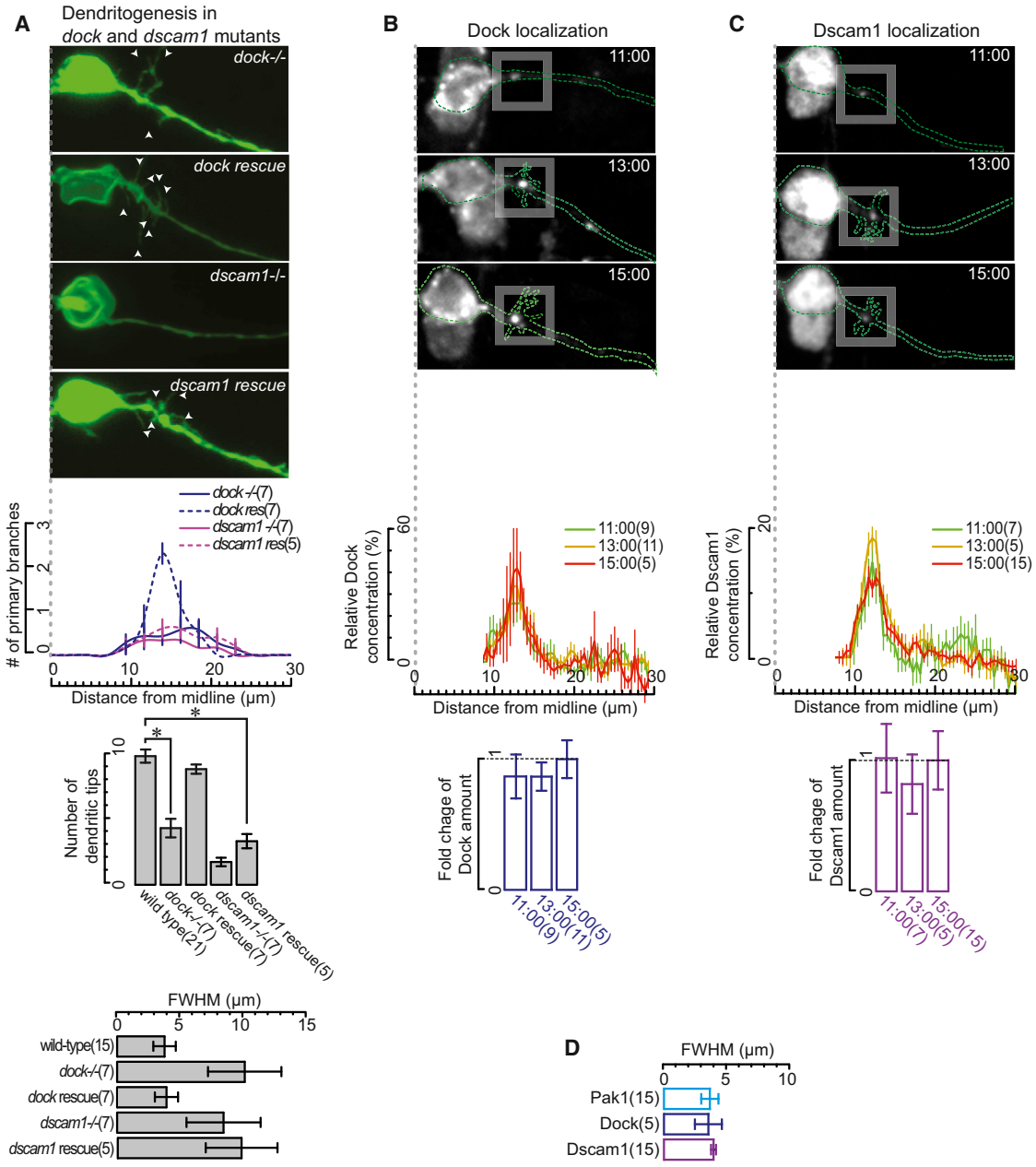

Figure 5. Dscam1 and Dock Are Localized at the aCC Dendritogenesis Site and Are Important for aCC Dendrite Outgrowth

(A) Images of aCC in indicated genotypes at 15:00. We also quantified the positions of primary dendritic branches, the numbers of dendritic tips, and the distribution FWHMs for the primary dendritic position in indicated genotypes at 15:00 (*$p < 0.005$ by one-way ANOVA).

(B and C) Images of Dscam1 and Dock distributions in aCC. Before aCC dendritogenesis starts at 11:00, Dock (B) and Dscam1 (C) are pre-localized at the aCC dendritogenesis site. The amounts of Dock and Dscam1 10 to 30 μm from the midline were also quantified from 11:00 to 15:00 and were normalized to the ones at 15:00.

(D) Comparison of the distribution FWHMs for Dscam1, Dock, and Pak1. Error bars, SEM.

See also Figures S4 and S5 and Table S1.

dscam1 RNAi but not in *pak*$^{-/-}$ embryos, whereas Dscam1 accumulation was not affected in either *dock*$^{-/-}$ or *pak*$^{-/-}$ embryos (Figure 6A). We also examined the pattern of Cdc42 activation in *dscam*$^{-/-}$ and *dock*$^{-/-}$ embryos using the aProbe reporter (Figure S6A). Neither the level of Cdc42 activation (Figure S6B) nor its spatial extent (Figure S6C) was affected. Together with the observation that Cdc42 activation occurs at a later time point than the accumulation of Dscam1, Dock, or Pak1 (i.e., it cannot be upstream of these three), we concluded that Cdc42 activation is controlled by a separate signaling pathway.

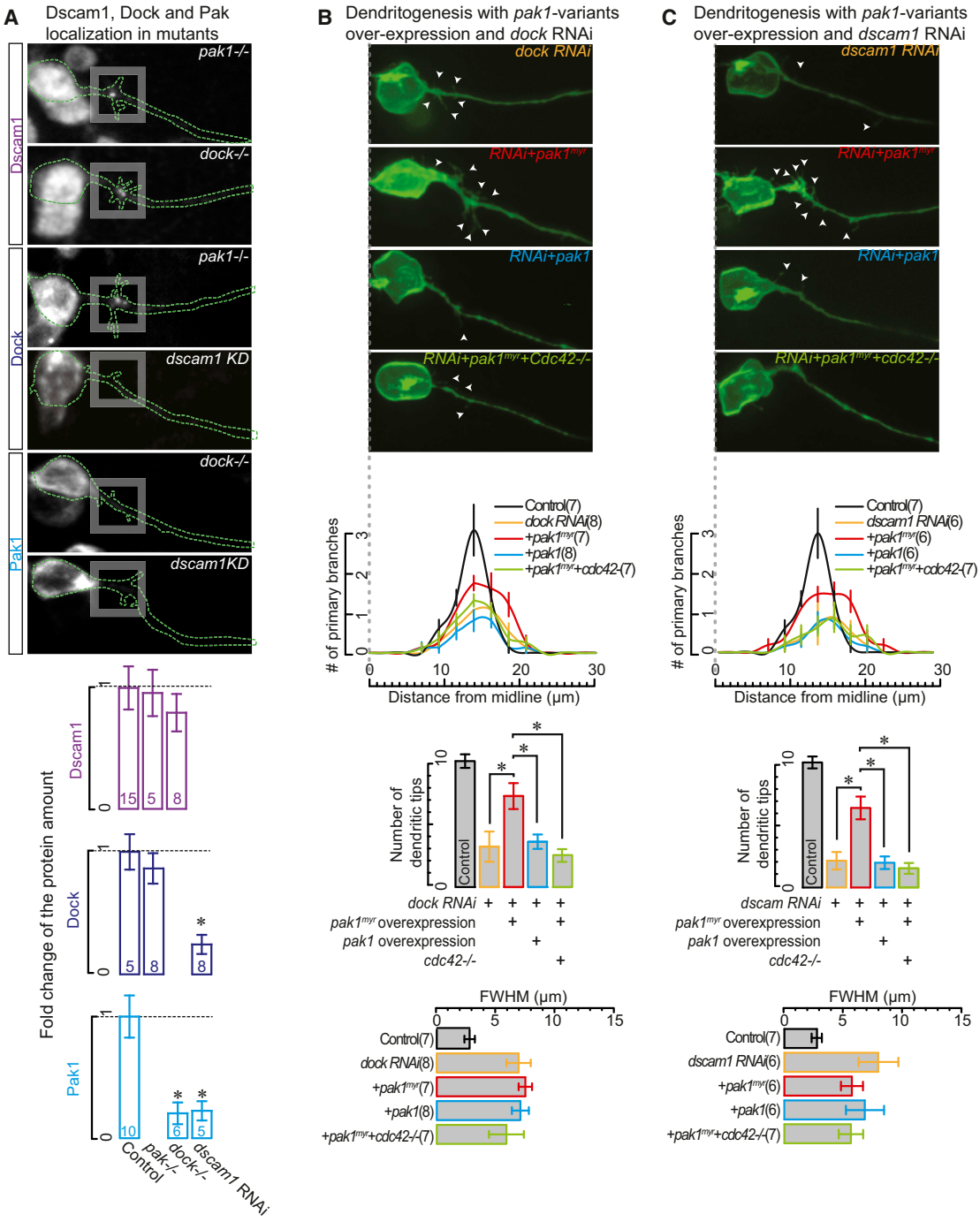

Figure 6. Dscam1 via Dock Localizes Pak1 at the aCC Dendritogenesis Site

(A) Images and quantifications of Dscam1, Dock, and Pak1 localized at the aCC dendritogenesis site in various mutant and knockdown backgrounds (*$p < 0.005$ compared with their amounts in a wild-type background at 15:00 by two-tailed t test).

(B and C) Images of aCC in indicated genotypes at 15:00. We also quantified the positions of primary dendritic branches, the numbers of dendritic tips, and the distribution FWHMs for the primary dendritic position in indicated genotypes at 15:00 (*$p < 0.005$ by one-way ANOVA). Error bars, SEM. Control data (*eve′-GAL4*$^{/+}$) from Figures 2B and 4A are replotted.

See also Figure S6 and Tables S1 and S2.

If Dscam1 and Dock act upstream of Pak1 to recruit Pak1 to the plasma membrane, Pak1^{myr} expression should override some aspects of the *dock* or *dscam1* mutant phenotype. To test this prediction, we analyzed aCC co-expressing Pak1^{myr} and shRNA of either *dock* or *dscam1* (Figures 6B and 6C) We verified that RNAi-mediated knocking down of *dock* or *dscam1*

displays a similar phenotype as in *dock*$^{-/-}$ or *dscam1*$^{-/-}$ null mutants, with a reduction in the dendrite tip number and misplacement of primary branches. The dendrite tip number reduction was significantly reversed by introducing Pak1^{myr}, although the region of the primary branches follows the broader Cdc42 activation pattern (compare Figure S6C to Figures 6B and 6C). The rescue of the dendrite tip number requires both Pak1 myristoylation and Cdc42 activation (Figures 6B and 6C). These data suggest that Dscam1, via Dock, recruits Pak1 to the plasma membrane to position the dendritogenesis site. Together with the activation of Cdc42, these two independent pathways co-regulate the initiation of dendrite growth in aCC.

Dscam1 in the MP1 Neuron Is Necessary and Sufficient in Signaling to Dscam1 in the aCC Neuron during aCC Dendritogenesis

Dscam1 has been shown to mediate contact repulsion through binding to Dscam1 itself (Wojtowicz et al., 2004, 2007) or guide axon growth through binding to Netrin (Andrews et al., 2008) in a context-dependent manner. We found no apparent dendrite phenotype in *netrin-A, netrin-B* double mutant embryos, whereas *dscam1* RNAi in all neurons excluding the aCC resulted in a drastic reduction in the number of dendritic tips (Figure S7A). The latter case is similar to our failed rescue by resupplying *dscam1* to aCC in the *dscam1*$^{-/-}$ background earlier in this paper. These results suggest that Dscam1 in another neuron is responsible, either directly or indirectly, for promoting dendrite outgrowth in aCC.

To identify the neuron in which *dscam1* is required for aCC dendritogenesis, we screened 20 *GAL4* lines driving *UAS-dscam1RNAi* in distinct subsets of neurons (Figure S7B). Among the 3 lines showing significant reduction of the aCC dendrite tip number, *R23E04-GAL4* is the only one that does not drive expression in aCC. Using this line to express membrane-tagged mCherry (*R23E04-GAL4*, *UAS-membrane-targeted mCherry*), we found that random 86%, 56%, and 10% fractions of the dMP2, MP1, and DO4 neurons, respectively, were labeled (n = 42 hemi-segments; Figure 7A and Figures S7C and S7D). In particular, the axon of the MP1 pioneer neuron crosses the aCC axon exactly at the dendritogenesis site (12.5 ± 0.5 μm from the midline for the aCC dendritogenesis site and 12.8 ± 0.2 μm for the MP1 axon; Figure 7A). At the crossing, these two axons have a center-to-center distance of 1.4 ± 0.3 μm (Figure 7A), matching their 1- to approximately 1.5-μm diameter and thus suggesting their direct contact. The MP1 axon starts crossing the ventral side of aCC from 10:00 to 10:30 AEL (Figure 7A). This timing is consistent with that for Dscam1, Dock, and Pak1 accumulation to occur in aCC, and the crossing direction matches the ventral-dorsal asymmetry of Pak1 and the primary dendrite branches around the aCC axon cross section (Figure 4). Therefore, MP1 is likely the partner neuron that supplies the ligand to Dscam1 in aCC.

To assess the role of MP1 Dscam1 in aCC dendritogenesis, we expressed *UAS-dscam1 RNAi* using *R23E04-GAL4* and marked aCC neurons with lipophilic dye. Because *R23E04-GAL4* is active only in a random half of MP1 neurons, we co-expressed *UAS-membrane-targeted-mCherry* as an expression marker (Figure 7B). In this case, mCherry-positive MP1 neurons would lose *dscam1* because of *dscam1*-RNAi expression. In their associated aCC neurons, we observed defects in dendrite growth (dendrite tip number of 3 ± 0.56, mean ± SEM). As an internal control, in the same embryos, dendrite growth in aCC neurons associated with mCherry-negative MP1 neurons (i.e., *dscam1* RNAi negative) was normal (dendrite tip number of 9.75 ± 0.32, compared to 9.49 ± 0.51 in *R23E04-GAL4*$^{/+}$, the control, with mean ± SEM; Figure 7B). We verified that the axon of RNAi-positive MP1 neurons retained their spatial relationship with aCC: neither their positions with respect to the midline nor their center-to-center distances to aCC axons were altered (Figure 7A). Therefore, the gross morphological change of the nervous system caused by *dscam1* malfunction (Schmucker et al., 2000) has not yet started to occur for MP1 at the developmental stage of our study. To rule out the possibility that our phenotype could be attributed to *dscam1* RNAi in other neurons where *R23E04-GAL4* was active, we identified another *GAL4* line (*C544-GAL4*) that drives expression specifically in MP1 (in a random half of all MP1 neurons). We observed the same dendritogenesis defect in aCC that runs across an MP1 axon expressing *dscam1* shRNA (dendrite tip number of 4 ± 0.38, mean ± SEM; Figures S7C and S7D). Taken together, these experiments demonstrated that *dscam1* specifically in MP1 is necessary to promote the branching of aCC dendrites.

We next sought to assess whether Dscam1 in MP1 is sufficient in signaling to Dscam1 in aCC. Because we did not observe substantial changes in MP1 morphology in *dscam1*$^{-/-}$ embryos at the developmental stage of our study (Figure S7F), we examined the aCC dendritogenesis phenotype when resupplying a single isoform of Dscam1 simultaneously to both MP1 and aCC using *R23E04-GAL4* and *eve′-GAL4* in *dscam1*$^{-/-}$ embryos. We observed a rescue of dendritogenesis in aCC associated with Dscam1-expressing MP1 (dendrite tip number of 7.3 ± 0.6, compared the control of 10.2 ± 0.75, mean ± SEM; Figure 7C) but not in those associated with MP1 not expressing Dscam1 (dendrite tip number of 1.7 ± 0.4, mean ± SEM; Figure 7C). Together with our failed rescue when resupplying the same isoform of *dscam1* only to aCC (Figure 5A), we argue that Dscam1 in MP1 is both necessary and sufficient in signaling to Dscam1 in aCC.

To provide direct evidence that Dscam1 in MP1 communicates to aCC, we imaged endogenous Dscam1 in MP1 using the GFP-nanobody method described earlier. By expressing mCherry::anti-GFP nanobody in *Dscam1*^{MiMICGFP} using *R23E04-GAL4*, we observed that Dscam1 in MP1 was enriched at the position where MP1 and aCC crossed (Figure 8A). We further examined whether *dscam1* RNAi in MP1 affects Dscam1 accumulation in aCC. To address this question, we imaged the accumulation of Dscam1 in aCC using the GFP-nanobody method. Because this method used both GFP and mCherry color channels, we were not able to mark MP1 neurons positive in *dscam1* RNAi. Nevertheless, we clearly saw a bimodal distribution of Dscam1 accumulation in aCC neurons (Figures 8B and 8C). In 52% of the aCC neurons, the mCherry nanobody at the dendrite growth site of aCC reduced to a level similar to that observed previously in aCC *dscam1* RNAi, whereas in other aCC neurons, Dscam1 accumulation was unaffected (Figure 8C). The fraction of affected aCC neurons matched the expected fraction of GAL4-active MP1 neurons (56%). These results strongly indicate that Dscam1 in MP1 is responsible for the

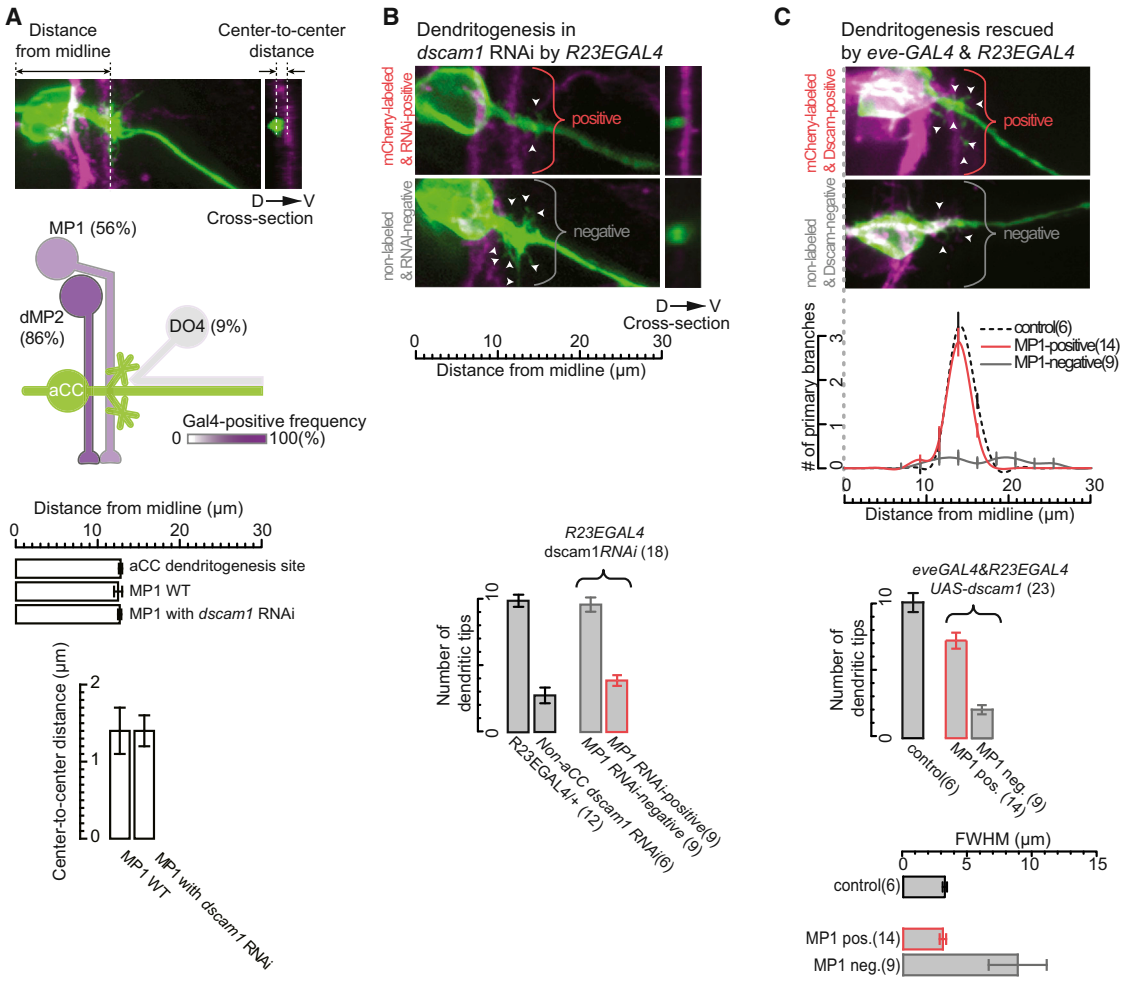

Figure 7. Dscam1 in the MP1 Neuron Is Necessary and Sufficient in Signaling to Dscam1 in the aCC Neuron during aCC Dendritogenesis

(A) Morphology of aCC (green) and neurons expressing membrane-bound mCherry (magenta) under the control of an *R23E04-GAL4* driver. mCherry-positive neurons appear in a patchy fashion in a small subset of neurons in the CNS. Among these neurons, MP1 has an axon positioned at close apposition of the aCC dendritogenesis site. MP1 projects its axon and crosses at the ventral side of aCC, where dendrites normally emerge (cross section). The position of the MP1 axon at the crossing site, as well as the MP1-aCC center-to-center distance, was unaffected by *dscam1* RNAi in MP1.

(B) Correlation between the presence of *dscam1*-RNAi-expressing MP1 and the loss of dendritic processes in aCC. The *dscam1*-RNAi-expressing MP1 has been labeled by mCherry (magenta) within the CNS of otherwise non-labeled and *R23E04-GAL4*$^{/+}$ animals.

(C) Rescue of the Dscam1 mutant phenotype by resupplying *dscam1* to both MP1 and aCC. The *dscam1*-expressing MP1 was labeled by mCherry (magenta). We quantified the positions of primary dendritic branches, the numbers of dendritic tips, and the distribution FWHMs for the primary dendritic position in indicated genotypes at 15:00. Here, *n* indicates the number of aCC analyzed in abdominal segments from A2 to A5. Error bars, SEM.

See also Figure S7 and Tables S1 and S3.

accumulation of Dscam1 in aCC at the neuron-neuron contact site, although they cannot tell whether there is direct Dscam1-Dscam1 interaction between the two neurons.

DISCUSSION

The precise positioning of dendritic arbors requires intricate communication between intracellular signaling and extracellular space. Here, using the *Drosophila* embryonic aCC motoneuron as the model system, we have elucidated a mechanism for cell-cell contact to specify the position of dendritogenesis (Figure 8D). In this mechanism, Dscam1 serves as the cell surface receptor, recruiting Dock and subsequently the Cdc42 effector Pak1 to the plasma membrane and thus channeling the signal from activated Cdc42 to a small region at the contact site. Our model is based on three sets of evidence.

Localized Dscam1-Dock-Pak1 Intracellular Signaling Defines the aCC Dendritogenesis Site

We have presented several lines of data showing that a signaling pathway from the surface protein Dscam1 to the intracellular protein Dock and then to Pak1 plays an important role in positioning the site of dendrite outgrowth. Our genetic studies showed that *dscam1*, *dock*, and *pak1* mutations all have a reduction of the aCC dendritic branch number and misplacement of the remaining branches. This pathway is cell autonomous for

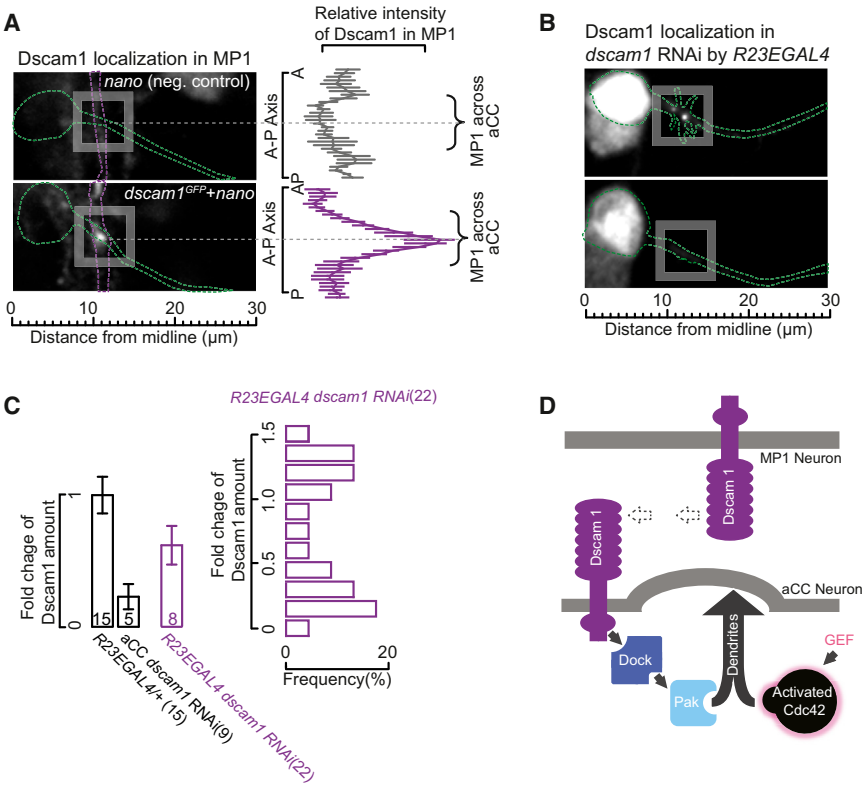

Figure 8. Dscam1 in MP1 Is Responsible for the Localization of Dscam1 in aCC

(A) Representative images of Dscam1 localized in MP1. The fluorescence intensity profiles were aligned and averaged at the aCC-MP1 intersection (dashed line).

(B) Representative images of Dscam1 in aCC in *dscam1* RNAi driven by the *R23E04-GAL4* driver.

(C) Quantification of Dscam1 accumulation in aCC (purple) displays a bimodal distribution, with the two populations matching that of the no-RNAi control and aCC *dscam1* RNAi (black). Here, *n* indicates the number of aCC analyzed in abdominal segments from A2 to A5. Error bars, SEM.

(D) Model for the spatial-temporal control of aCC dendritogenesis.

aCC because aCC-specific RNAi of *dscam1*, *dock*, and *pak1* displayed the same dendrite loss and misplacement, and resupplying *dock* or *pak1* to aCC in the corresponding mutant background rescues the phenotype. As a separate piece of evidence, our imaging experiments showed that Dscam1, Dock, and Pak1 are accumulated at the aCC dendritogenesis site at least 2 hr before the initiation of dendrites, with the position and spatial extent of their accumulation precisely matching that of aCC primary dendritic branches. Imaging results under aCC-specific RNAi establish a Dscam1-Dock-Pak1 hierarchy, because knocking down any one of these genes disrupts the accumulation of downstream partners but not that of upstream ones. We validated this pathway by examining a *pak1* allele that disrupts its interaction with *dock*, as well as by analyzing genetic interaction. This pathway is consistent with previous biochemical studies that have shown interactions among Dscam1, Dock, and Pak1 in vitro (Hing et al., 1999; Schmucker et al., 2000). While these previous studies pointed to the role of this interaction in regulating axonal guidance, our study has clearly demonstrated a mechanism for this Dscam signaling in modulating dendrite morphogenesis by coupling to cytoskeleton activity regulation.

Cdc42 Activation and Membrane Enrichment of Pak1 Are Independent Signals Controlling the Timing and Spatial Extent of aCC Dendritogenesis, Respectively

Our genetic and imaging data have provided strong evidence that the activation of Cdc42 and the membrane enrichment of Pak1 are independent of each other: Pak1 accumulation occurs 2 hr before Cdc42 activation, whereas Cdc42 activation is normal in *dscam1* and *dock* mutants that disrupt Pak1 accumulation. This mechanism differs from a canonical model of Pak1 membrane localization, in which activated Cdc42 becomes membrane-anchored through lipid modification, subsequently recruiting and activating Pak1 (Etienne-Manneville, 2004; Park and Bi, 2007; Slaughter et al., 2009). In contrast, our observation suggests that the recruitment of Pak1 to the target site, through Dscam1 and Dock, is decoupled from the control of Cdc42 activation by GEFs and GAPs. Moreover, we have seen a substantially narrower spatial extent for Pak1 accumulation than that for Cdc42 activation, matching that of primary dendrite branches. Therefore, in controlling aCC dendritogenesis, Pak1 is not purely a downstream effector of Cdc42 but also an input point to supply a spatial cue. Nevertheless, the activation of Pak1 requires Cdc42, because dendrite growth does not occur before the time point of Cdc42 activation. In addition, our study does not rule out the possibility for feedback loops to be subsequently involved to refine the region where Cdc42 is activated (Goryachev and Pokhilko, 2008).

Our high-resolution SIM images showed that Pak1 is recruited not just to a segment of the aCC axon near the dendritogenesis site but more specifically to the ventral-side plasma membrane where dendrite outgrowth occurs. This phenomenon is consistent with Dscam1 being a transmembrane protein, and it indicates the role of Pak1 membrane recruitment in channeling the Cdc42 signal to a precise location. As a cytoplasmic protein, enriching Pak1 on the plasma membrane would lead to higher local concentration and thus more efficient coupling with activated, membrane-anchored Cdc42 (Bishop and Hall, 2000; Burbelo et al., 1995). Consistent with this model, direct tethering of Pak1 to the plasma membrane by overexpressing $Pak1^{myr}$ (but not by overexpressing wild-type Pak1) overrides the spatial confinement of dendrite outgrowth. Primary dendrite branches now spread over the whole region where Cdc42 is activated, while dendritogenesis timing is still set by Cdc42 activation. This membrane-enrichment model could represent a generic mechanism for Rho-GTPase-mediated cytoskeletal activity to

accept multiple inputs. Specifically in our system of aCC dendritogenesis, this mechanism allows the positioning and timing of the event to be independently specified, and dendrite outgrowth initiates when and where Cdc42 activation and Pak1 membrane localization coincide.

The independence of Cdc42 activation and the Dscam1-Dock-Pak1 pathway also explains why any one of the *dscam1*, *dock*, or *pak1* mutants does not fully abolish dendrite growth but shows reduced dendrite branch numbers. In these mutants, Cdc42 still activates normally. Therefore, it can still activate Pak1 (except in the case of the *pak1* mutant) and other Cdc42 effectors. Nevertheless, the efficiency will be lower without these effectors being enriched at the plasma membrane, leading to a reduction of dendritogenesis activity. In addition, the loss of spatial input causes expansion of the dendrite growth region to match the region of Cdc42 activation.

Dscam1 Signaling in aCC Is Positioned by aCC-MP1 Neuron-Neuron Contact

One of our interesting findings is the role of the MP1 pioneering neuron in positioning aCC dendrites. Our imaging experiment revealed that MP1 projects its axon around 10:00 AEL across the ventral side of aCC. The crossing position is the same location where Pak1 accumulates in aCC and where dendrite outgrowth occurs later. Previous serial sectioning electron microscopy confirms this observation and shows that MP1 and aCC make neuron-neuron contact at this position (Jacobs and Goodman, 1989). This finding resembles recent studies of axon collateral branching of a *C. elegans* hermaphrodite-specific neuron, in which cell-cell contact allows the SYG-2 ligand in hypodermis cells to signal the SYG-1 receptor in the neuron. A WAVE regulatory complex (WRC) interacting receptor sequence in the SYG-1 cytoplasmic tail subsequently recruits WRC, a well-known downstream effector of Rac that regulates actin assembly, triggering axon branching (Chia et al., 2014). In our case, it appeared that Dscam1 acts on both sides of the neuron-neuron contact. A convincing piece of evidence came from the mosaic RNAi of *dscam1* in MP1 using both the *R23E04-GAL4* line and the MP1-specific *C544-GAL4* line. In the same embryos, it showed perfect correlation between MP1 *dscam1* RNAi expression and loss of aCC Dscam1 accumulation, as well as reduction of aCC dendrites. We have verified that *dscam1* RNAi did not change the spatial relationship between MP1 and aCC at the developmental stage of our study. Therefore, the observed aCC dendrite phenotype was not due to the misplacement of the MP1 axon. We further demonstrated that resupplying *dscam1* to both MP1 and aCC was sufficient to substantially rescue the aCC loss-of-dendrite phenotype in *dscam1*$^{-/-}$ flies. Finally, we showed that endogenous Dscam1 in MP1 accumulated at the site where the MP1 axon crossed aCC. All these results support our claim that Dscam1 in MP1 directly provides the positional cue for Dscam1 signaling in aCC dendritogenesis.

Because of the complicated nature of the Dscam1-Dscam1 interaction, clarifying whether Dscam1 in aCC and MP1 interacts directly or indirectly is beyond the scope of this paper. Stochastic Dscam1 alternative splicing (Miura et al., 2013; Neves et al., 2004; Zhan et al., 2004) means that it is unlikely for aCC and MP1 to have completely matching Dscam1 splicing variants for homophilic or other isoform-specific interactions. Alternatively, communication between Dscam1 on the two sides of the MP1-aCC contact could be mediated by a co-receptor that is yet to be identified.

In either case, our key discovery elucidates a mechanism by which Dscam1 regulates cytoskeleton dynamics by bringing specific effectors to the plasma membrane of the action site. We have shown that this mechanism is important for spatial specification of the dendritogenesis site in the aCC neuron, while similar processes might be involved in other cases in which neuron-neuron recognition is translated into CNS morphogenesis, including the self-avoidance of dendrites from the same neuron (Hughes et al., 2007; Matthews et al., 2007; Soba et al., 2007). In these cases, the exact neuron behavior triggered by Dscam1 signaling will depend not only on the input received by Dscam1 but also on the local molecular context.

EXPERIMENTAL PROCEDURES

Generation of Transgenic Lines

All constructs used were generated using standard cloning procedures. All constructs were further cloned into a standard P-element transformation vector pUASt or a PhiC31 integrase-mediated transformation vector pACU (gifts from Y.N. Jan). For details, refer to the Supplemental Experimental Procedures. Transformants of all constructs were established at Genetic Services. Except for the *mCherry::anti-GFP nanobody* lines and the *CD8::SNAP* line (see Table S1 for the site-specific locations), all fly lines were generated by random transgene insertion through the P-element transposon technology. This random insertion allowed us to select for clonal lines with a very low expression level. These low-expression lines were used in all experiments to minimize overexpression artifacts.

Fly Stocks

A detailed description of all fly stocks, crosses, and transgenes used can be found in the Supplemental Experimental Procedures and Table S1. Flies were reared at 25°C using standard procedures.

Generation and Visualization of Dscam1^{GFPMiMIC}

The following injections were done to generate EGFP-tagged *dscam1*: the *phiC31;Mi{MIC}Dscam1*$^{MI07658/+}$ embryos were injected with *pBS-KS-attB1-2-PT-SA-SD-2-tdEGFP* (a modified protein trap vector from *pBS-KS-attB1-2-PT-SA-SD-2-EGFP-FlAsH-StrepII-TEV-3xFlag*; Venken et al., 2011). Transformants were identified by the absence of the yellow gene. The transformants are homozygous viable, and the expression matched that of the endogenous Dscam1 (Figure S4B), indicating that introduction of the tag into the endogenous locus does not grossly disrupt the gene function.

RNAi Experiments

Following an hour of collection, embryos were injected individually with dsRNA constructs prepared against *Drosophila* homologs of CRIB proteins. These dsRNA constructs were synthesized using the MEGAscript T7 Transcription Kit (Life Technologies). For cell-specific RNAi experiments, we obtained the *UAS-shRNA* lines from the Transgenic RNAi Project (TRiP) at Harvard Medical School and the Vienna *Drosophila* RNAi Center. For examination of *dscam1* functions outside of the aCC, we expressed a *dscam1* RNAi construct in various small subset of neurons (*UAS-CD4::tdTomato*$^{/+}$*;UAS-dscam1RNAi/GAL4 driver*). See the Supplemental Experimental Procedures and Tables S2 and S3 for details.

Immunohistochemistry

Embryos were fillet dissected, fixed with 4% paraformaldehyde for 10 min, and blocked in a solution of PBS/0.01% TritonX with 3% BSA (TBSB) for 1 hr. The embryos were incubated with primary antibodies or BG-Alexa645/TBSB (a final concentration of 100 nM; NEB) at 4°C overnight. Subsequently, they were stained with the proper secondary antibodies for 2 hr at 23–25°C.

Following immunohistochemistry, they were post-fixed with 4% paraformaldehyde for 5 min and mounted in ProLong Gold anti-fade mountant (Invitrogen). See the Supplemental Experimental Procedures for a complete list of primary and secondary antibodies used in this study.

Imaging

The 3D image data from multiple samples (*n*) of the model neuron were compiled and quantified. Fluorescent images were collected from immunostained embryos using a confocal microscope and a structured illumination microscope. Detailed methods for imaging are described in the Supplemental Experimental Procedures.

Imaging Analysis

Images were analyzed using ImageJ. Figures were prepared using Adobe Photoshop and Illustrator. Statistics were calculated using Origin. For details of quantifying dendritic processes, aCC and MP1 position, fluorescently tagged protein concentration, and Pak membrane localization, see the Supplemental Experimental Procedures.

SUPPLEMENTAL INFORMATION

Supplemental Information includes Supplemental Experimental Procedures, seven figures, and three tables and can be found with this article online at http://dx.doi.org/10.1016/j.devcel.2015.09.007.

ACKNOWLEDGMENTS

We thank G.J. Bashaw, S. Crew, C. Desai, R. Fehon, M. Fujioka, H. Hing, Y.N. Jan, T. Lee, J. Wang, L. Zipursky, TRiP at Harvard Medical School, the Vienna Drosophila RNAi Center, the Bloomington Drosophila Stock Center (BDSC), the Drosophila Genomics Resource Center, the Berkeley Drosophila Genome project, and the Developmental Studies Hybridoma Bank (DSHB) for fly strains, antibodies, and plasmids. We are grateful to G. Izaguirre and D. Gorczyca for technical assistance; V. Mennella for help with SIM imaging; T. Kidd, V. Lemmon, and T. Uemura for helpful discussion; and Y.N. Jan for thoughtful comments on the manuscript. This work was supported by funding from NIH/NIMH R21MH101688 (to B.H. and D.K.) and the Searle Scholarship, Packard Fellowship in Science and Engineering (to B.H.).

Received: April 2, 2015
Revised: July 7, 2015
Accepted: September 11, 2015
Published: October 12, 2015

REFERENCES

Aceto, D., Beers, M., and Kemphues, K.J. (2006). Interaction of PAR-6 with CDC-42 is required for maintenance but not establishment of PAR asymmetry in *C. elegans*. Dev. Biol. *299*, 386–397.

Alberts, B. (1998). The cell as a collection of protein machines: preparing the next generation of molecular biologists. Cell *92*, 291–294.

Alberts, B., Johnson, A., Lewis, J., Raff, M., Roberts, K., and Walter, P. (2007). Molecular Biology of the Cell, Fifth Edition (Garland Science).

Andrews, G.L., Tanglao, S., Farmer, W.T., Morin, S., Brotman, S., Berberoglu, M.A., Price, H., Fernandez, G.C., Mastick, G.S., Charron, F., and Kidd, T. (2008). Dscam guides embryonic axons by Netrin-dependent and -independent functions. Development *135*, 3839–3848.

Bishop, A.L., and Hall, A. (2000). Rho GTPases and their effector proteins. Biochem. J. *348*, 241–255.

Bokoch, G.M. (2003). Biology of the p21-activated kinases. Annu. Rev. Biochem. *72*, 743–781.

Burbelo, P.D., Drechsel, D., and Hall, A. (1995). A conserved binding motif defines numerous candidate target proteins for both Cdc42 and Rac GTPases. J. Biol. Chem. *270*, 29071–29074.

Cheng, P.L., and Poo, M.M. (2012). Early events in axon/dendrite polarization. Annu. Rev. Neurosci. *35*, 181–201.

Chia, P.H., Chen, B., Li, P., Rosen, M.K., and Shen, K. (2014). Local F-actin network links synapse formation and axon branching. Cell *156*, 208–220.

Dickson, B.J. (2002). Molecular mechanisms of axon guidance. Science *298*, 1959–1964.

Dong, X., Liu, O.W., Howell, A.S., and Shen, K. (2013). An extracellular adhesion molecule complex patterns dendritic branching and morphogenesis. Cell *155*, 296–307.

Dong, X., Shen, K., and Bülow, H.E. (2015). Intrinsic and extrinsic mechanisms of dendritic morphogenesis. Annu. Rev. Physiol. *77*, 271–300.

Etienne-Manneville, S. (2004). Cdc42—the centre of polarity. J. Cell Sci. *117*, 1291–1300.

Etienne-Manneville, S., and Hall, A. (2002). Rho GTPases in cell biology. Nature *420*, 629–635.

Formstecher, E., Aresta, S., Collura, V., Hamburger, A., Meil, A., Trehin, A., Reverdy, C., Betin, V., Maire, S., Brun, C., et al. (2005). Protein interaction mapping: a *Drosophila* case study. Genome Res. *15*, 376–384.

Garvalov, B.K., Flynn, K.C., Neukirchen, D., Meyn, L., Teusch, N., Wu, X., Brakebusch, C., Bamburg, J.R., and Bradke, F. (2007). Cdc42 regulates cofilin during the establishment of neuronal polarity. J. Neurosci. *27*, 13117–13129.

Goryachev, A.B., and Pokhilko, A.V. (2008). Dynamics of Cdc42 network embodies a Turing-type mechanism of yeast cell polarity. FEBS Lett. *582*, 1437–1443.

Govek, E.E., Newey, S.E., and Van Aelst, L. (2005). The role of the Rho GTPases in neuronal development. Genes Dev. *19*, 1–49.

Govek, E.E., Hatten, M.E., and Van Aelst, L. (2011). The role of Rho GTPase proteins in CNS neuronal migration. Dev. Neurobiol. *71*, 528–553.

Gustafsson, M.G., Shao, L., Carlton, P.M., Wang, C.J., Golubovskaya, I.N., Cande, W.Z., Agard, D.A., and Sedat, J.W. (2008). Three-dimensional resolution doubling in wide-field fluorescence microscopy by structured illumination. Biophys. J. *94*, 4957–4970.

Hall, A. (1998). Rho GTPases and the actin cytoskeleton. Science *279*, 509–514.

Hall, A., and Lalli, G. (2010). Rho and Ras GTPases in axon growth, guidance, and branching. Cold Spring Harb. Perspect. Biol. *2*, a001818.

Heintzmann, R., and Gustafsson, M.G.L. (2009). Subdiffraction resolution in continuous samples. Nat. Photonics *3*, 362–364.

Hing, H., Xiao, J., Harden, N., Lim, L., and Zipursky, S.L. (1999). Pak functions downstream of Dock to regulate photoreceptor axon guidance in *Drosophila*. Cell *97*, 853–863.

Hsu, S.N., Yonekura, S., Ting, C.Y., Robertson, H.M., Iwai, Y., Uemura, T., Lee, C.H., and Chiba, A. (2009). Conserved alternative splicing and expression patterns of arthropod N-cadherin. PLoS Genet. *5*, e1000441.

Hughes, M.E., Bortnick, R., Tsubouchi, A., Bäumer, P., Kondo, M., Uemura, T., and Schmucker, D. (2007). Homophilic Dscam interactions control complex dendrite morphogenesis. Neuron *54*, 417–427.

Jacobs, J.R., and Goodman, C.S. (1989). Embryonic development of axon pathways in the *Drosophila* CNS. II. Behavior of pioneer growth cones. J. Neurosci. *9*, 2412–2422.

Jan, Y.N., and Jan, L.Y. (2003). The control of dendrite development. Neuron *40*, 229–242.

Jan, Y.N., and Jan, L.Y. (2010). Branching out: mechanisms of dendritic arborization. Nat. Rev. Neurosci. *11*, 316–328.

Kamiyama, D., and Chiba, A. (2009). Endogenous activation patterns of Cdc42 GTPase within *Drosophila* embryos. Science *324*, 1338–1340.

Kennerdell, J.R., and Carthew, R.W. (1998). Use of dsRNA-mediated genetic interference to demonstrate that frizzled and frizzled 2 act in the wingless pathway. Cell *95*, 1017–1026.

Kozubowski, L., Saito, K., Johnson, J.M., Howell, A.S., Zyla, T.R., and Lew, D.J. (2008). Symmetry-breaking polarization driven by a Cdc42p GEF-PAK complex. Curr. Biol. *18*, 1719–1726.

Lichtman, J.W., and Denk, W. (2011). The big and the small: challenges of imaging the brain's circuits. Science *334*, 618–623.

Lu, W., Katz, S., Gupta, R., and Mayer, B.J. (1997). Activation of Pak by membrane localization mediated by an SH3 domain from the adaptor protein Nck. Curr. Biol. *7*, 85–94.

Luo, L. (2000). Rho GTPases in neuronal morphogenesis. Nat. Rev. Neurosci. *1*, 173–180.

Manser, E., Leung, T., Salihuddin, H., Zhao, Z.S., and Lim, L. (1994). A brain serine/threonine protein kinase activated by Cdc42 and Rac1. Nature *367*, 40–46.

Matthews, B.J., Kim, M.E., Flanagan, J.J., Hattori, D., Clemens, J.C., Zipursky, S.L., and Grueber, W.B. (2007). Dendrite self-avoidance is controlled by Dscam. Cell *129*, 593–604.

McGorty, R., Kamiyama, D., and Huang, B. (2013). Active microscope stabilization in three dimensions using image correlation. Opt. Nanoscopy *2*, 1–13.

Miura, S.K., Martins, A., Zhang, K.X., Graveley, B.R., and Zipursky, S.L. (2013). Probabilistic splicing of Dscam1 establishes identity at the level of single neurons. Cell *155*, 1166–1177.

Mogilner, A., Allard, J., and Wollman, R. (2012). Cell polarity: quantitative modeling as a tool in cell biology. Science *336*, 175–179.

Murakoshi, H., Wang, H., and Yasuda, R. (2011). Local, persistent activation of Rho GTPases during plasticity of single dendritic spines. Nature *472*, 100–104.

Neves, G., Zucker, J., Daly, M., and Chess, A. (2004). Stochastic yet biased expression of multiple Dscam splice variants by individual cells. Nat. Genet. *36*, 240–246.

Owen, D., Mott, H.R., Laue, E.D., and Lowe, P.N. (2000). Residues in Cdc42 that specify binding to individual CRIB effector proteins. Biochemistry *39*, 1243–1250.

Park, H.O., and Bi, E. (2007). Central roles of small GTPases in the development of cell polarity in yeast and beyond. Microbiol. Mol. Biol. Rev. *71*, 48–96.

Salzberg, Y., Díaz-Balzac, C.A., Ramirez-Suarez, N.J., Attreed, M., Tecle, E., Desbois, M., Kaprielian, Z., and Bülow, H.E. (2013). Skin-derived cues control arborization of sensory dendrites in *Caenorhabditis elegans*. Cell *155*, 308–320.

Sanes, J.R., and Zipursky, S.L. (2010). Design principles of insect and vertebrate visual systems. Neuron *66*, 15–36.

Schmucker, D., Clemens, J.C., Shu, H., Worby, C.A., Xiao, J., Muda, M., Dixon, J.E., and Zipursky, S.L. (2000). *Drosophila* Dscam is an axon guidance receptor exhibiting extraordinary molecular diversity. Cell *101*, 671–684.

Slaughter, B.D., Smith, S.E., and Li, R. (2009). Symmetry breaking in the life cycle of the budding yeast. Cold Spring Harb. Perspect. Biol. *1*, a003384.

Soba, P., Zhu, S., Emoto, K., Younger, S., Yang, S.J., Yu, H.H., Lee, T., Jan, L.Y., and Jan, Y.N. (2007). *Drosophila* sensory neurons require Dscam for dendritic self-avoidance and proper dendritic field organization. Neuron *54*, 403–416.

Venken, K.J., Schulze, K.L., Haelterman, N.A., Pan, H., He, Y., Evans-Holm, M., Carlson, J.W., Levis, R.W., Spradling, A.C., Hoskins, R.A., and Bellen, H.J. (2011). MiMIC: a highly versatile transposon insertion resource for engineering *Drosophila melanogaster* genes. Nat. Methods *8*, 737–743.

Vitriol, E.A., and Zheng, J.Q. (2012). Growth cone travel in space and time: the cellular ensemble of cytoskeleton, adhesion, and membrane. Neuron *73*, 1068–1081.

Wang, J., Ma, X., Yang, J.S., Zheng, X., Zugates, C.T., Lee, C.H., and Lee, T. (2004). Transmembrane/juxtamembrane domain-dependent Dscam distribution and function during mushroom body neuronal morphogenesis. Neuron *43*, 663–672.

Welch, C.M., Elliott, H., Danuser, G., and Hahn, K.M. (2011). Imaging the coordination of multiple signalling activities in living cells. Nat. Rev. Mol. Cell Biol. *12*, 749–756.

Wojtowicz, W.M., Flanagan, J.J., Millard, S.S., Zipursky, S.L., and Clemens, J.C. (2004). Alternative splicing of *Drosophila* Dscam generates axon guidance receptors that exhibit isoform-specific homophilic binding. Cell *118*, 619–633.

Wojtowicz, W.M., Wu, W., Andre, I., Qian, B., Baker, D., and Zipursky, S.L. (2007). A vast repertoire of Dscam binding specificities arises from modular interactions of variable Ig domains. Cell *130*, 1134–1145.

Yogev, S., and Shen, K. (2014). Cellular and molecular mechanisms of synaptic specificity. Annu. Rev. Cell Dev. Biol. *30*, 417–437.

Zhan, X.L., Clemens, J.C., Neves, G., Hattori, D., Flanagan, J.J., Hummel, T., Vasconcelos, M.L., Chess, A., and Zipursky, S.L. (2004). Analysis of Dscam diversity in regulating axon guidance in *Drosophila* mushroom bodies. Neuron *43*, 673–686.